

Theoretical Uncertainties in Red Giant Branch Evolution: The Red Giant Branch Bump

Stephan R. Bjork and Brian Chaboyer

Department of Physics and Astronomy, Dartmouth College, 6127 Wilder Lab, Hanover, NH 03755

Brian.Chaboyer@Dartmouth.edu

ABSTRACT

A Monte Carlo simulation exploring uncertainties in standard stellar evolution theory on the red giant branch of metal-poor globular clusters has been conducted. Confidence limits are derived on the absolute V -band magnitude of the bump in the red giant branch luminosity function ($M_{V,b}$) and the excess number of stars in the bump, R_b . The analysis takes into account uncertainties in the primordial helium abundance, abundance of alpha-capture elements, radiative and conductive opacities, nuclear reaction rates, neutrino energy losses, the treatments of diffusion and convection, the surface boundary conditions, and color transformations.

The uncertainty in theoretical values for the red giant bump magnitude varies with metallicity between $+0.13/ - 0.12$ mag at $[\text{Fe}/\text{H}] = -2.4$ and $+0.23/ - 0.21$ mag at $[\text{Fe}/\text{H}] = -1.0$. The dominant sources of uncertainty are the abundance of the alpha-capture elements, the mixing length, and the low-temperature opacities. The theoretical values of $M_{V,b}$ are in good agreement with observations. The uncertainty in the theoretical value of R_b is ± 0.01 at all metallicities studied. The dominant sources of uncertainty are the abundance of the alpha-capture elements, the mixing length, and the high-temperature opacities. The median value of R_b varies from 0.44 at $[\text{Fe}/\text{H}] = -2.4$ to 0.50 at $[\text{Fe}/\text{H}] = -1.0$. These theoretical values for R_b are in agreement with observations.

Subject headings: globular clusters: general — stars: evolution — stars: interiors — stars: luminosity function

1. Introduction

Globular clusters are made up of a very large number of stars with varying mass but identical age, composition, and distance. This makes them a rich and productive application of the theory of stellar structure and evolution. Detailed stellar evolution calculations are done numerically using computer programs which incorporate previously calculated nuclear reaction rates and opacities, approximations to complex phenomena such as convection, and assumptions about the chemical

composition. To compare theoretical models to observations, moreover, requires converting physical quantities such as luminosity and surface temperature to the observational system of magnitudes and colors using empirical relations or the results of separate stellar atmosphere models. The results of theoretical stellar evolution calculations, therefore, depend upon a set of prior assumptions. To assess the reliability of theoretical models of globular clusters stars one must study how uncertainties in these assumptions of stellar evolution theory propagate to the predictions of the theory.

In this work we are interested specifically in studying uncertainties in stellar evolution theory along the red giant branch (RGB) of metal-poor globular clusters. The RGB is the region in a color-magnitude diagram comprising low-mass stars that have already expended the hydrogen fuel at their center, and are burning hydrogen in a spherical shell around an inert helium core. Stars in this stage of evolution grow larger, brighter, and redder over time. An excellent review of RGB evolution is found in Salaris, Cassisi & Weiss (2002), including a discussion of uncertainties in the theoretical models and observational tests of the theory. Much of our work was guided by this review.

After a low-mass star has consumed all the hydrogen at its center, the envelope of the star expands and it moves across the color-magnitude diagram from the main sequence region towards lower effective temperature and redder colors. Stars in this stage are said to be on the subgiant branch. Initially, hydrogen burning continues through a thick shell covering a region of mass $\sim 0.1M_{\odot}$, while outside the hydrogen-burning shell the stellar envelope has the original chemical composition with a convective region in the star’s outer layers. As the star progresses along the subgiant branch, the hydrogen-burning shell narrows to a mass of $\sim 0.001M_{\odot}$ while the convective region grows steadily deeper. The convective region eventually reaches material previously processed by the hydrogen-burning core during the main sequence phase, and containing a higher abundance of helium which immediately is mixed throughout the convective region.

Eventually, the stellar luminosity begins to grow as the effective temperature continues to drop, and the star is said to be at the base of the RGB. The star progresses up the RGB as the hydrogen-burning shell moves outward through the star leaving behind an increasingly massive core of helium. The star’s radius continues to grow larger, its effective temperature lower, and its luminosity brighter. The lower boundary of the convective region, which reached a maximum depth near the base of the RGB, recedes steadily.

A discontinuity in the chemical composition is left at the maximum depth reached by the convective envelope, since convection mixes hydrogen from the envelope into the partially depleted region left behind by the hydrogen-burning core of the main sequence phase. When the hydrogen-burning shell reaches this discontinuity, the sudden increase in available fuel causes the stellar luminosity to drop temporarily, and the star’s evolution pauses before continuing its progression up the RGB. This point is called the RGB bump.

There is a very strong correlation between stellar luminosity and the mass of the helium core along the RGB. The luminosity grows as the core mass grows, and since the rate at which mass is

added to the helium core is itself proportional to the luminosity, this means that throughout red giant evolution the helium core mass and the luminosity increase at an ever faster rate. The one exception to this is at the RGB bump, where the sudden change in chemical composition causes the growth in luminosity to pause temporarily, while the helium core continues to gain mass.

The probability of observing a star in a given luminosity range on the RGB is inversely proportional to the rate at which stars evolve at that luminosity. In observed globular cluster color-magnitude diagrams, therefore, we find that the number of observed stars steadily decreases along the RGB, except at the red giant bump. In fact, the differential luminosity function of a globular cluster, showing the number N of observed stars as a function of magnitude, descends along the RGB as a nearly straight line in the magnitude- $\log N$ plane. The slope of this line indicates how the rate of evolution increases along the RGB.

Globular cluster luminosity functions provide an important test of the accuracy of stellar evolution models. The number of stars observed as a function of luminosity indicates the relative timescale of stellar evolution, which in turn conveys information about the internal chemical structure of stars. A great deal of attention has been paid, for example, to the total number of stars on the RGB compared to the main sequence turn-off region. Several authors (Bolte 1994; Vandenberg, Larson & de Propris 1998; Langer, Bolte & Sandquist 2000) have found a discrepancy in this quantity between observed luminosity functions for the globular clusters M5 and M30 and the predictions of stellar evolution theory. Vandenberg, Larson & de Propris (1998) take this discrepancy to suggest the presence of rapidly rotating cores in red giants, while Langer, Bolte & Sandquist (2000) take it to indicate the possibility of a chemical mixing process deep in the stellar interior.

The magnitude of the RGB bump in observed globular clusters serves to indicate the depth of the chemical discontinuity left by the convective envelope at its point of deepest extent near the base of the RGB. In one of the first extensive studies of the red giant bump, Fusi Pecci et al. (1990) compared observational determinations of the bump magnitude in 11 globular clusters to theoretical predictions. They found that, taken relative to the horizontal branch magnitude, theoretical values of the bump magnitude are higher than observed values by about 0.4 mag. However, more recent studies using updated stellar evolution models and improved observations (Cassisi & Salaris 1997; Zoccali et al. 1999; Riello et al. 2003) have found no discrepancy between theory and observations.

Cassisi & Salaris (1997) have studied how uncertainties in the most important individual stellar evolution parameters impact the magnitude of the red giant bump. They look at the equation of state, mixing length, mass loss along the RGB, opacities, and the V -band bolometric correction. In addition, Cassisi, degl’Innocenti & Salaris (1997) studied the impact of element diffusion in detail. The effects of overshooting from the convective envelope have been considered by Alongi et al. (1991). This paper presents a comprehensive study of $M_{V,b}$ incorporating all the relevant uncertainties to firmly establish the agreement between standard stellar models and observations of the red giant bump.

The magnitude of the RGB bump depends upon critically upon the maximum depth of the

convection zone. In contrast, the enhancement in the observed number of stars in the bump depends upon the size of the chemical discontinuity. Bono et al. (2001) introduced the R_b parameter, which measures the relative number of stars in the RGB bump. Bono et al. (2001) found that R_b was a robust prediction of stellar evolution theory, as changes in the opacity, equation of state, and nuclear cross sections changed the predicted value of R_b by a few percent. Their work found fair agreement between the observed R_b values and those predicted by standard stellar evolution theory. More recently Riello et al. (2003) used HST data to determine R_b in 54 Galactic globular clusters. They found this data was in good agreement with standard stellar evolution models.

This paper presents a comprehensive analysis of how uncertainties in the inputs into stellar evolution theory effect the predictions for $M_{V,b}$ and R_b . Section 2 provides an overall of the Monte Carlo approach used in the paper, while §3 presents a detailed analysis of the uncertainties in standard stellar evolution theory. The theoretical luminosity functions are presented in §4. Section 5 discusses the $M_{V,b}$ results, while the R_b results are presented in §6. A summary of the main results is given in §7.

2. Method

Since it is not feasible to use analytic error propagation formulas with the complex calculations of stellar evolution, one must use numerical methods to study how uncertainty in the parameters of stellar evolution theory propagate to the predictions of the theory. A simple approach is to consider one parameter at a time, performing calculations with several different values of the parameter to examine how the predictions of the theory are affected (e.g. Castellani & degl’Innocenti 1999). The effects involved are generally small, so changes in the parameters produce a roughly linear response in results of the calculations. However, this method does not describe how uncertainties in many different parameters interact to produce a combined uncertainty in the predictions of the theory. To investigate this requires a larger set of calculations, in which all of the significant parameters vary simultaneously.

We use a Monte Carlo approach to the problem. Describing the estimated uncertainty in each parameter with a probability distribution, we run a large number of independent stellar evolution calculations in which the value of each parameter is drawn randomly from its corresponding probability distribution. For specific quantitative predictions of the theory, then, the results of all the runs can be combined into histograms showing the most probable value and the distribution of uncertainty around it. This method has been used previously in a series of papers examining uncertainties in theoretical globular cluster ages (Chaboyer et al. 1996, 1998; Chaboyer & Krauss 2002; Krauss & Chaboyer 2003). The work here is essentially an extension of this method to study theoretical uncertainties in RGB evolution.

Stellar evolution is strongly affected by the abundance of heavy elements in a star, indicated by the relative iron abundance $[Fe/H]$. Because the iron abundance (or metallicity) of a star can be

determined from observations, it is treated as a known quantity in our simulation rather than as a source of theoretical uncertainty. We therefore conduct our analysis at five different metallicity values spanning a range typical of old galactic globular clusters. For each set of randomly generated parameters in the Monte Carlo simulation, we calculate an evolutionary sequence using $[\text{Fe}/\text{H}] = -1.0, -1.3, -1.6, -2.0, \text{ and } -2.4$. The results are analyzed separately for each metallicity.

Our stellar evolution calculations are made using the Dartmouth stellar evolution program (Chaboyer et al. 2001), which is a descendant of the Yale Rotating Stellar Evolution Code (Guenther et al. 1992). To explore the evolution of metal-poor stars along the RGB, we calculated evolutionary sequences for a variety of masses and metallicities starting from previously constructed zero-age main sequence models. Evolution was carried up to the tip of the RGB, which we defined as the point where energy generated by the triple-alpha reaction reached 1% of the star’s total luminosity. The equations of stellar structure were solved to an accuracy of a few parts in 10^5 . With these tolerances, the code requires about 6000 – 7500 individual stellar models to evolve the highest metallicity stars to the tip of the RGB, and for the lowest metallicity stars it requires 3500 – 4000 models. Each stellar model comprises about 600 spherical shells on the main sequence, and approximately 1500 shells along the RGB. The greatest difficulty in the Monte Carlo approach is that it is computationally very demanding. This study required 45,000 evolutionary sequences, roughly 230 billion stellar models, and approximately 600 CPU days on a Beowulf cluster of 2.0Ghz Athalon processors.

In all the stellar evolution calculations we use the standard DSEP equation of state, which includes the Debye-Hückel correction of Clayton (1968) for electrostatic interactions in the fully ionized plasma. The DSEP equation of state in the fully ionized regime ($T > 10^6$ K) is essentially the relativistic ideal gas law with the electrostatic interaction, radiation pressure, and electron degeneracy effects included. In the partially ionized regime it is a Saha equation including single ionization of hydrogen and metals, and double ionization of helium. Although a more sophisticated equation of state is now available in the OPAL tables of Rogers (1994), Chaboyer & Kim (1995) have found that using the OPAL tables in place of the standard DSEP equation of state does not change the evolution of metal-poor stars significantly. Based on their work, we consider the equation of state to be an insignificant source of uncertainty in metal-poor red giant evolution.

Similarly, all of our calculations use the standard treatments of Salpeter (1954) and Graboske et al. (1973) to evaluate plasma screening effects on the nuclear reactions. More recent treatments of plasma screening are available (e.g., Mitler 1977). However, Cassisi et al. (1998) report that their numerical experiments found the new formulations to have no impact on metal-poor red giant evolution. We therefore do not consider plasma screening as a source of uncertainty.

The other important parameters of stellar evolution theory—opacities, nuclear reaction rates, composition, surface boundary conditions, neutrino cooling rates, and the treatments of convection and diffusion—represent possible sources of uncertainty, and so they are varied throughout the Monte Carlo simulation. The treatment of these parameters is detailed in the next section.

3. Sources of Uncertainty

There are 18 parameters of stellar evolution theory that we consider as possibly significant sources of uncertainty. Some of these, like the primordial helium abundance, are simple numerical values that vary through the Monte Carlo simulation. Others, though, like the opacities and nuclear reaction rates, enter the stellar evolution calculations as tables or formulas. These quantities are varied by multiplying the table or formula by an overall coefficient, and then varying the coefficient through the Monte Carlo simulation. In the case of high-temperature opacities, we use different but correlated multiplicative factors in different regions of the table. For the bolometric corrections, which are logarithmic quantities, we add rather than multiply by an overall uncertainty term.

During the Monte Carlo simulation, the value of each parameter is drawn randomly from a probability density distribution that we choose to reflect the estimated uncertainty in the parameter. In general, we use Gaussian distributions to reflect uncertainties that are statistical in nature, with a well-defined most probable value. For systematic uncertainties we use uniform distributions in which the probability density is constant within some range and zero outside of it. For the surface boundary conditions there are two independent formulations to choose from, and here we use a binary distribution in which one or the other formulation is chosen with equal probability.

The 18 parameters varied in the Monte Carlo simulation are listed in Table 1 along with the probability density distributions used in the Monte Carlo simulation. In many cases, we adopt a distribution from one of the previous papers in which Monte Carlo simulations were used to investigate stellar evolution models at the main sequence turn-off point and on the subgiant branch (Chaboyer et al. 1996, 1998; Chaboyer & Krauss 2002; Krauss & Chaboyer 2003). For others, we review the literature directly to estimate an appropriate distribution, and these are discussed in detail.

Convective overshoot. One of the weaknesses of the mixing length approximation used in standard stellar evolution models is that it fails to properly describe the boundary between convective and radiative regions in a star. Assuming no composition gradient, this boundary is established by the Schwarzschild condition as the point where the temperature gradient in the star is equal to the adiabatic temperature gradient. The mixing length approximation assumes that all convective motion is confined to this region of instability.

In reality, convective material reaches the boundary of the unstable region with a non-zero velocity, and therefore tends to penetrate across the Schwarzschild boundary into the stable radiative region. This phenomenon is called convective overshoot, and it has been demonstrated in hydrodynamical simulations of convection (e.g., Singh, Roxburgh & Chan 1998). The extent to which overshooting actually occurs in stars, however, is unclear.

Since the stars in our simulation do not have convective cores, we are concerned only with overshooting at the base of the surface convection zone. The stellar evolution calculations model convective overshooting by assuming that the region in which the chemical composition is homog-

enized by convective mixing extends some distance below the Schwarzschild boundary into the stable radiative region. Temperature gradients, however, are taken to be unaffected by overshooting. The single parameter in this treatment is the depth by which convective mixing reaches into the radiative region, and this distance is expressed as a fraction of the pressure scale height at the Schwarzschild boundary.

An upper limit on convective overshooting in metal-poor stars is set by observed lithium abundances. Lithium breaks down in the high temperatures of stellar interiors, beginning near the bottom of the surface convection zone. A large amount of convective overshooting would carry lithium more quickly from the surface to the interior, and lithium depletion would occur at a faster rate. Overshooting depths greater than about $0.2 H_p$ would be inconsistent with the relatively high lithium abundances observed in metal-poor stars. In our simulation, therefore, we draw values for the overshooting depth from the uniform distribution $0.0 - 0.2 H_p$.

Diffusion coefficients. Models of stable astrophysical plasmas predict that helium and heavy elements in a star’s radiative regions should settle toward the center of the star over time, while hydrogen rises toward the surface. The extent to which this actually occurs, however, is subject to considerable uncertainty. There is clear evidence from helioseismology that element diffusion occurs in the sun (Christensen-Dalsgaard, Proffitt & Thompson 1993; Basu, Pinsonneault & Bahcall 2000). Studies of surface abundances in metal-poor stars, though, indicate that in these stars diffusion for some reason does not occur in the outer layers (Chaboyer et al. 2001).

Our stellar evolution calculations incorporate element diffusion using the treatment of Thoul, Bahcall & Loeb (1994). Because diffusion is not seen in the outer layers of metal-poor stars, we include a modification introduced by Chaboyer et al. (2001) which suppresses diffusion near the surface. By comparing observed iron abundances in globular clusters to the iron abundance predicted by their stellar evolution models, Chaboyer et al. (2001) estimate that whatever process inhibits diffusion in metal-poor stars must act over an outer region of at least $0.005 M_\odot$. On the other hand, the fact that diffusion is not found to be inhibited in the sun suggests that the process inhibiting diffusion extends no lower than the bottom of the solar surface convection zone, which has a mass of $0.02 M_\odot$. Therefore Chaboyer et al. conclude that the process inhibiting diffusion likely acts over a surface region with mass somewhere between 0.005 and $0.02 M_\odot$.

To reflect this in our calculations we follow Chaboyer et al. (2001) in setting the diffusion coefficients to zero in the outer $0.005 M_\odot$ layer of the star. In the interior region defined by $M_* - M(r) > 0.02 M_\odot$ where M_* is the star’s total mass, the diffusion coefficients are set to the standard values of Thoul, Bahcall & Loeb (1994). In the middle region $0.005 M_\odot < M_* - M(r) < 0.02 M_\odot$, the coefficients are ramped from zero to the standard values.

To reflect the uncertainty in this treatment of diffusion, we multiply the diffusion coefficients overall by a factor drawn from the uniform distribution $0.5 - 1.3$. This range is chosen based on an estimated 30% uncertainty in the theoretical calculations of diffusion velocities (see e.g. Chaboyer et al. 1996), but the lower end of the range is extended to account for the fact that several physical

processes in the interior of a star might slow the rate of diffusion, while no such processes would increase it.

Triple-alpha reaction rate. The point at which helium ignition occurs in a star’s evolution depends on the rate of the helium-burning triple-alpha reaction, in which three helium nuclei fuse to form a single nuclei of ^{12}C . Our calculations use the rate of Caughlan & Fowler (1988), with an uncertainty estimated at 15% (e.g. Castellani & degl’Innocenti 1999). We therefore multiply the standard Caughlan & Fowler (1988) rate by a factor drawn from the Gaussian distribution 1.00 ± 0.15 .

Plasma neutrino cooling rate. Neutrino cooling in the stellar core becomes an important effect in the evolution of stars on the upper RGB. Energy lost through the emission of neutrinos tends to slow the rise in temperature as the helium core grows, allowing the core to reach a higher mass before helium burning begins. Significant energy loss can occur through several different neutrino processes in a stellar plasma; for the helium core of stars on the upper RGB the most important is the plasma process, in which a plasmon (a quantized electromagnetic oscillation in the plasma) spontaneously decays into a neutrino-antineutrino pair (Itoh et al. 1996).

We use the plasma neutrino cooling rates of Haft, Raffelt & Weiss (1994), who have calculated numerical rates based on the treatment of electromagnetic dispersion relations in plasmas provided by Braaten & Segel (1993), and have also derived an analytic approximation to the numerical results for use in stellar evolution calculations. They find their analytic approximation accurate to within 4% in regimes where the plasma process is dominant and within 5% everywhere.

Published neutrino cooling rates are generally calculated under the standard assumption that neutrinos have no magnetic dipole moment. A non-zero magnetic moment for neutrinos would tend to increase the plasma neutrino emission rates and could impact stellar evolution significantly. In fact, Raffelt (1990); Raffelt & Weiss (1992) and Castellani & degl’Innocenti (1993) have used stellar evolution calculations incorporating a non-zero neutrino magnetic moment to constrain the magnetic moment through comparison to globular cluster observations.

Although the existence of a non-zero magnetic moment could significantly impact stellar evolution at the tip of the RGB, this possibility is considered at the moment to be outside of standard physics, and so we do not incorporate it into our analysis. Instead, we consider the error in the Haft, Raffelt & Weiss (1994) analytic approximation formula to be the dominant source of uncertainty in the neutrino cooling rates, and to reflect this in the Monte Carlo simulation we multiply the Haft, Raffelt & Weiss formula by a factor drawn from the Gaussian distribution 1.00 ± 0.05 .

Conductive opacities. In the deep interior of RGB stars, thermal conduction by electrons serves as an important means of energy transfer. The thermal conductivity under these conditions therefore serves to establish the temperature gradient in red giant interiors and determine when the core becomes hot enough to ignite helium.

Conductive opacities are one of the most significant sources of uncertainty on the upper RGB,

so a close examination of our current understanding in this area is appropriate. There are essentially two treatments of conductive opacity available for use in red giant models: the tabulated values of Hubbard & Lampe (1969) and the more recent calculations of Itoh et al. (1983). However, as Catelan et al. (1996) point out, the Itoh et al. (1983) calculations were made for conditions characteristic of white dwarfs and neutron stars; red giant cores do not fall within their range of validity. Specifically, the Itoh et al. results are presented as an analytic fitting formula in terms of the parameter

$$\Gamma = \frac{Z^2 e^2}{r k_B T}$$

which characterizes the strength of the electrostatic interaction between ions in a plasma. Here e is the electron charge, Z is the atomic number, k_B is the Boltzmann constant, and $r = [3/(4\pi n_i)]^{1/3}$ is the ion-sphere radius with n_i the number density of ions. The domain where $2 \lesssim \Gamma \lesssim 171$ represents matter in the liquid metal phase, while $\Gamma \lesssim 2$ corresponds more typically to a Boltzmann gas. The fitting formula of Itoh et al. (1983) intended for application to dense matter in the liquid metal phase, is valid only in the range $2 \leq \Gamma \leq 160$, while in red giant cores Γ is considerably lower. Applying the results of Itoh et al. (1983) to RGB stars therefore requires extrapolating the fitting formula from liquid metal conditions to Boltzmann gas conditions, and it is not clear how much error this extrapolation introduces. Because of this, Catelan et al. (1996) conclude that the Hubbard & Lampe (1969) values are to be preferred at present.

The treatment of conductive opacity in our stellar evolution calculations is based on the Hubbard & Lampe (1969) tables, along with the relativistic extension provided by Canuto (1970) for higher densities. Specifically, we employ a set of analytic fitting formulas from Sweigart (1973); for $\log \rho \leq 5.8$, we use Sweigart’s fit to the Hubbard & Lampe tables, while for $\log \rho \geq 6.0$ we use Sweigart’s fit to the Canuto relativistic opacities. For $5.8 < \log \rho < 6.0$ we use a ramp between the non-relativistic and relativistic formulas, also provided by Sweigart (1973). For conditions appropriate to red giant stars, we find that Sweigart’s formula are accurate to about 10% when compared to the Hubbard & Lampe (1969) tabulations.

We estimated the uncertainty in conductive opacities by directly comparing values from the Itoh et al. (1983) analytic formula to the tabulated values of Hubbard & Lampe (1969). Catelan et al. (1996) have plotted both these sets of opacities for conditions typical of red giant cores. Their plot shows that here the Itoh et al. values run $\sim 10 - 30\%$ lower than the Hubbard & Lampe values. Since the Itoh et al. fitting formula was not designed to be accurate in this regime, though, it is possible that this comparison could exaggerate the difference between the two treatments. To check this, we also compared the two sets of opacities in a density-temperature region where both treatments are valid.

We make the comparison at densities typical of red giant cores ($\rho \sim 10^5 - 10^6 \text{ g/cm}^3$). The acceptable temperature range is then bounded by two restrictions in the Itoh et al. (1983) analysis. On the upper end there is the restriction that $\Gamma > 2$. On the lower end is the requirement that a high-temperature classical limit apply to the treatment of the ionic system. This is expressed by

the condition $y \ll 1$ where the parameter y is defined

$$y \equiv \frac{\hbar^2 k_F^2}{2Mk_B T}$$

with k_F being the Fermi wavenumber of the electrons and M the mass of an ion. Mitake, Ichimaru & Itoh (1984) found that the high-temperature classical limit is adequate as long as $y < 0.01$. In the range $0.01 < y < 0.1$, though, their results show that a quantum correction not included in the Itoh et al. (1983) analysis tends to reduce the conductive opacities by up to 25%.

In Figure 1 we have plotted the conductive opacities at densities of $10^{5.0}$ and $10^{5.5}$ g/cm³ for temperatures where $\Gamma > 2$ and $y < 0.1$, and we show the temperatures corresponding to $y = 0.01$. The agreement between the different treatments is better at the higher temperatures, where the classical treatment of ions by Itoh et al. is most valid and also where the temperatures approach those typically found in red giant cores ($T \sim 10^{7.5} - 10^{8.0}$ K). In the region where $y < 0.01$ the treatments agree to within 25%, with the Itoh et al. values running 5 – 25% below the Hubbard & Lampe (1969) values.

Taking all of this into consideration, we estimate that current values for the conductive opacity in red giant cores are uncertain by about 20% at the 1- σ level. We therefore multiply our standard values (obtained as described above from Sweigart’s fit to the Hubbard & Lampe tables and the relativistic Canuto treatment) by a factor drawn from the Gaussian distribution $1.00 \pm .20$.

Bolometric corrections. In order to compare our stellar evolution models to observations, it is necessary to transform the physical quantities used in stellar evolution calculations to those quantities measured by observers. Specifically, we must transform the theoretically calculated bolometric luminosity, effective temperature, and surface gravity to predict the observational magnitudes for specific pass bands. Generally, this transformation is made using color tables based on theoretical treatments of stellar atmospheres, possibly calibrated by empirical data. Purely empirical relationships between magnitude and effective temperature are also available based on effective temperatures measured for nearby stars, but these relationships are valid only for a restricted range of metallicities and evolutionary stages.

The transformations used in our analysis are based on the color tables constructed for the Revised Yale Isochrones (Green, Demarque & King 1987). These transformations are an empirical recalibration of the theoretical colors and bolometric corrections of Vandenberg & Bell (1985) and Kurucz (1979). In this study we will examine the V -band magnitude of the RGB bump, so we must estimate the uncertainty in the V -band bolometric corrections. Weiss & Salaris (1999) compare the V -band bolometric corrections (BC_V) from several theoretical, empirical, and semi-empirical sources and find that with a consistent choice for the solar BC_V , all the sources agree to within 0.05 mag along a typical globular cluster isochrone. Our own analysis of different (BC_V) from different sources confirm this result. Therefore, for BC_V , we draw the uncertainty term from the uniform distribution ± 0.05 mag.

4. Theoretical Luminosity Functions

To explore uncertainties in $M_{V,b}$ and R_b , we conducted a Monte Carlo simulation with 1120 independent sets of randomly chosen stellar evolution parameters, from each set generating luminosity functions at several different metallicities, ages, and assumed initial mass functions.

Generating luminosity functions requires a series of theoretical evolutionary tracks calculated for stars over a range of masses. In this work we use the nine masses $M = 0.55, 0.63, 0.70, 0.75, 0.80, 0.85, 0.90, 0.95,$ and $1.00 M_\odot$. Each evolutionary track is calculated from the zero-age main sequence to the tip of the RGB. The range of masses was chosen to allow reliable luminosity functions for ages between 10 and 20 Gigayears.

From a set of evolutionary tracks at appropriate masses one can calculate theoretical isochrones at a variety of ages. We use a modified version of the isochrone generating program used to construct the Revised Yale Isochrones (Green, Demarque & King 1987). The program uses the method of equivalent evolutionary points, locating in each evolutionary track a set of points defined in terms of the central helium abundance (on the main sequence) or the helium core mass (on the RGB) and interpolating among them to generate the isochrones. From these isochrones, V -band luminosity functions are calculated. Uncertainty in the bolometric correction is incorporated at a later stage of the analysis. Luminosity functions are normalized to 1000 stars on the zero-age main sequence and use a bin size of 0.04 mag.

Generating a luminosity function requires an initial mass function (IMF) describing the relative number of stars as a function of mass created during the formation of the cluster. The IMF is generally assumed to have the form of a simple declining power law, $\xi(M) \propto M^{-\alpha}$. In the classic study, Salpeter (1955) found that observational data suggested an initial mass function with exponent $\alpha = 2.35$; more recent studies, though, find evidence that the initial mass function for globular clusters varies from cluster to cluster and that metal-poor clusters in general have less steep IMFs than metal-rich clusters.

Because stars on the RGB represent a narrow range of masses, though, the luminosity function in the red giant region is less affected by the IMF than are the main sequence and subgiant branch. In particular, we expect that $M_{V,b}$ and R_b will be unaffected by the IMF. This is tested by generating luminosity functions using the Salpeter (1955) value for the IMF exponent as well as values from extremes of the reasonable range: $\alpha = 0.00, 2.35,$ and 4.00 .

Sample luminosity functions are shown in Figure 2. These luminosity functions were calculated using values for the stellar evolution parameters from the center of the uncertainty ranges discussed in Section 3. Luminosity functions are shown for a single metallicity at ages of 11, 13, and 15 Gigayears using the Salpeter value for the IMF exponent, $\alpha = 2.35$. The entire set of Monte Carlo luminosity functions (1140) for a Salpeter IMF, an age of 13 Gyr and $[\text{Fe}/\text{H}] = -2.4$ and $[\text{Fe}/\text{H}] = -1.0$ are shown in Figure 3. In making this figure, the luminosity functions have been normalized so that they all have the same number of stars at $M_V = 5.5$, which is approximately

1.5 mag below the turn-off.

5. The Magnitude of the Giant Branch Bump

To precisely locate the peak of the RGB bump in our calculated luminosity functions, we find the point in the luminosity function which corresponds to the most populated bin in the bump region, and then calculate the parabola passing through that point and the adjacent points on either side. The vertex of the parabola is taken as the peak of the bump, and the magnitude of the vertex as the bump magnitude.

As discussed in Section 3, the uncertainties in the Green, Demarque & King (1987) bolometric corrections taken into consideration by adding to the bump magnitude a term drawn randomly from the uniform range 0.00 ± 0.05 mag. For each of the 1120 Monte Carlo realizations at a given age and metallicity we generate ten such uncertainty terms, so that 1120 independent luminosity functions are used to produce 11,200 realizations of the bump magnitude. These realizations are independent in the bolometric correction, though not in other stellar evolution parameters. The increase in the number of points does not significantly improve the numerical accuracy of the Monte Carlo simulation, but it does provide smoother histograms.

Studies of the RGB bump (e.g. Fusi Pecci et al. 1990) often focus on the difference in magnitude between the bump and the zero-age horizontal branch level, $\Delta V_{\text{HB}}^{\text{bump}} = V_{\text{bump}} - V_{\text{HB}}$. Observationally, this quantity is more reliable than V_{bump} since it avoids uncertainties in the distance modulus and in the calibration of observational data. The theoretical evaluation of $\Delta V_{\text{HB}}^{\text{bump}}$, however, is subject to uncertainties in the luminosity of the horizontal branch. In order to confine our analysis to uncertainties on the RGB, we will consider the absolute magnitude M_V of the RGB bump rather than $\Delta V_{\text{HB}}^{\text{bump}}$.

Table 2 shows the median values of the bump magnitude obtained in the Monte Carlo simulation, along with 68% and 95% confidence limits. Both the median values and the confidence limits depend strongly on the cluster metallicity. In contrast, the choice of cluster age serves merely to shift the distributions of bump magnitude without affecting their shape, so the same confidence limits apply at all ages. In order to show the shape of the bump magnitude distributions, we plot the results for age 13 Gigayears as histograms in Figure 4.

Both Table 2 and Figure 4 show that the uncertainty in theoretical determinations of the bump magnitude increases with metallicity. At $[\text{Fe}/\text{H}] = -1.0$ the distribution of bump magnitudes obtained in the Monte Carlo simulation is about 80% wider than at $[\text{Fe}/\text{H}] = -2.4$. At all metallicities the distributions show a slight asymmetry, falling off more gradually toward dimmer magnitudes.

The effect of cluster age on the bump magnitude is essentially the same at all metallicities. An increase of 1 Gigayear in age corresponds to a shift towards dimmer bump magnitudes of $0.03 - 0.04$ mag, not a large effect compared to the width of the magnitude distributions. Even at the

lowest metallicity, where uncertainties in stellar evolution theory leave the tightest distribution of bump magnitudes, the shift in magnitude between age 11 Gyr and age 15 Gyr is only 60% of the distribution width at the 68% confidence level.

The effect of metallicity on the bump magnitude is much more significant. Changing the cluster metallicity by ± 0.1 to 0.2 dex leads to a shift in the bump magnitude comparable to the 68% theoretical confidence limits in Table 2. Since observational measurements of $[\text{Fe}/\text{H}]$ are uncertain by about ± 0.15 dex, this means that when we compare observational and theoretical determinations of the bump magnitude the uncertainties in stellar evolution theory are about as important as observational uncertainties in the metallicity scale.

Figure 5 shows the bump magnitude as a function of metallicity, compared to other theoretical and observational results. Error bars are shown representing the 68% confidence limits at age 13 Gyr, but we omit the error bars at ages 11 and 15 Gyr for clarity. The theoretical relation of Cassisi & Salaris (1997) for clusters of age 15 Gigayears is also shown, as well as observational results for 19 galactic globular clusters drawn from Zoccali et al. (1999). Cassisi & Salaris present their results in terms of the global metallicity $[\text{M}/\text{H}]$, and they assume a different value than we do for the solar heavy element abundance Z_{\odot} . To make their treatment of metallicity agree with ours, we shift their results to the $[\text{Fe}/\text{H}]$ scale assuming $[\alpha/\text{Fe}] = 0.45$ (the median value in our Monte Carlo simulation) and $Z_{\odot} = 0.018$. The Cassisi & Salaris relation is somewhat lower than our results for age 15 Gyr, especially at the highest and lowest metallicities. The difference, however, is well within the theoretical uncertainties.

The Zoccali et al. (1999) data points show the M_V -band magnitude of the red giant bump in 19 Galactic globular clusters observed with the *Hubble Space Telescope*. We use the Zinn & West (1984) metallicities for each cluster, and convert from apparent to absolute magnitude using the RR Lyrae calibration of Krauss & Chaboyer (2003): $M_V(\text{RR}) = 0.46 + 0.23([\text{Fe}/\text{H}] + 1.9)$. The uncertainty in the absolute magnitude of the bump is dominated by an uncertainty of ± 0.12 mag in the RR Lyrae calibration, while the uncertainty in globular cluster metallicities is about ± 0.15 dex.

The agreement between the Zoccali et al. (1999) observations and our theoretical models is excellent. Zoccali et al. themselves found a good agreement between their observational values of $\Delta V_{\text{HB}}^{\text{bump}}$ and the models of Cassisi & Salaris (1997) assuming an alpha-capture overabundance $[\alpha/\text{Fe}] = 0.30$ for $[\text{Fe}/\text{H}] < -1.0$. Our results show, similarly, a good agreement between observations and theoretical values of V_{bump} calculated with a median alpha-capture overabundance $[\alpha/\text{Fe}] = 0.45$. Moreover, the results of our Monte Carlo uncertainty analysis show that differences between theoretical and observed values of the bump magnitude lie within the theoretical uncertainties in stellar evolution as well as within the observational uncertainties in the globular cluster distance modulus and the metallicity scale. It is clear that there is currently no discrepancy between the V -band bump magnitude as observed in Galactic globular clusters and as calculated in standard stellar evolution models.

To analyze the individual influence of each continuously varying stellar evolution parameter on $M_{V,b}$, all 1120 Monte Carlo realizations are plotted on a graph of $M_{V,b}$ versus parameter value. The dependence of $M_{V,b}$ on a given parameter value is then characterized with a straight line fit. Specifically, the parameter range is divided into 20 bins containing 56 Monte Carlo realizations each, and for each bin the median value of $M_{V,b}$ and the 68% confidence limits are determined. A straight line is fit to the median points of each bin using the simple least-squares method with each bin weighted equally. Straight lines are also fit to the upper and lower 68% confidence points in each bin. Table 3 presents the slope of the linear dependence for the most significant stellar evolution parameters as well as the total change in bump magnitude as the parameter varies across its range of uncertainty, either between the endpoints of a uniform distribution or between the 68% confidence limits of a Gaussian distribution. The impact of surface boundary conditions is explored by comparing the Monte Carlo distribution of bump magnitudes obtained using the Eddington $T(\tau)$ relation to that using the Krishna-Swamy (1966) relation, and Table 3 records the difference between the median bump magnitudes obtained with each of the two treatments.

The three most significant sources of uncertainty in the bump magnitude are the alpha-capture abundance, the mixing length, and the low-temperature opacities. All three of these parameters have a stronger influence at higher metallicities, which explains why the overall uncertainty in the bump magnitude increases with metallicity. Other significant sources of uncertainty are the surface boundary conditions, convective overshoot, the $^{13}\text{C} + p \rightarrow ^{14}\text{N} + \gamma$ reaction rate, and the helium diffusion coefficients. The impact of these parameters does not vary significantly with $[\text{Fe}/\text{H}]$, and so the values given in Table 3 are averaged across all five metallicities. All of the other stellar evolution parameters explored in the Monte Carlo simulation are negligible, impacting the bump magnitude at the level of 0.05 mag or less.

Cassisi & Salaris (1997) and Cassisi, degl’Innocenti & Salaris (1997) have already studied the impact of a few of these stellar evolution parameters on theoretical bump magnitudes. Exploring the influence of mixing length, Cassisi & Salaris find a dependence $\Delta V_{\text{bump}}/\Delta \text{ml} \approx -0.27$ mag with Δml in units of H_p and with the metallicity unspecified, a result that is in rough agreement with our more detailed analysis. Cassisi, degl’Innocenti & Salaris (1997) consider the impact of diffusion on the bump luminosity, and find that including helium and heavy element diffusion according to the Thoul, Bahcall & Loeb (1994) coefficients lowers the bump luminosity by $\Delta V_{\text{bump}} \approx 0.07$ mag compared to models with no diffusion. The impact of diffusion in our Monte Carlo simulation is comparable.

It is interesting that convective overshoot represents only a secondary source of uncertainty in the bump magnitude. After one of the first studies of the RGB bump (Fusi Pecci et al. 1990) found a substantial discrepancy of 0.4 mag between observational and theoretical determinations of $\Delta V_{\text{hb}}^{\text{bump}}$, Alongi et al. (1991) suggested that this discrepancy could be resolved by including convective overshoot with extension $0.7 H_p$ in the theoretical models. More recent comparisons using newer observations and theoretical models (Cassisi & Salaris 1997; Zoccali et al. 1999) have found that the discrepancy is resolved even without convective overshoot. In addition, though, our

results show that with an upper limit of $0.2 H_p$ set by observed lithium abundances in metal-poor stars, the question of whether to include convective overshoot in stellar evolution models is in fact of only secondary importance, much less significant than the alpha-capture abundance, mixing length, and low-temperature opacities.

Finally, we consider the confidence limits in the bump magnitude obtained when the most significant parameters are held fixed at the center of their uncertainty range, indicating the accuracy that theoretical bump magnitudes would have if one of the important stellar evolution parameters were known precisely. Table 4 shows the 68% confidence limits for fixed values of the alpha-capture overabundance, mixing length, and low-temperature opacities. The median bump magnitudes in Table 2 for each metallicity and age still apply. Particularly important are the confidence limits obtained for fixed values of $[\alpha/\text{Fe}]$, both because this parameter is the greatest source of uncertainty and because it is in principle an observable quantity. The confidence limits in Table 4 indicate that if the alpha-capture abundance could be precisely determined for a given cluster, the uncertainty in the theoretical bump magnitude for that cluster would be reduced by about 35%. Improved spectroscopic observations of globular clusters allowing direct measurements of the alpha-capture abundance will therefore be the most important step toward improving the accuracy of theoretical bump magnitudes.

6. Number Counts of Stars in the Bump

The relative enhancement of the number of stars in the RGB bump can be measured using the R_b parameter introduced by Bono et al. (2001). It measures the relative evolutionary timescale for stars in the bump region to stars on the RGB which have not yet reached the bump region. The R_b parameter was measured in each of the MC luminosity functions, using the definition of Bono et al. (2001): the ratio between the star counts in the bump region $V_{\text{bump}} \pm 0.4 \text{ mag}$ to the star counts fainter on the RGB: $V_{\text{bump}} + 0.5 < V_{\text{bump}} < V_{\text{bump}} + 1.5$. In agreement with Bono et al. (2001) we find that R_b is a robust prediction of stellar evolution theory, with little uncertainty. The R_b parameter has a small dependence on $[\text{Fe}/\text{H}]$ and age, and the results from the MC simulation are summarized in Table 5. It was found that, at a given $[\text{Fe}/\text{H}]$ and age, the 1σ uncertainty in the prediction of R_b is ± 0.01 . Parameters which effect R_b the most are, in order of significance, $[\alpha/\text{Fe}]$, mixing length, the high temperature opacities, helium diffusion and the low temperature opacities. The relatively modest effect of each of these parameters on R_b is summarized in Table 6.

Comparison between observed and predicated values of R_b serves as an excellent test of standard stellar evolution theory. Riello et al. (2003) used HST data to determine R_b in 54 Galactic globular clusters, of which 40 are metal-poor ($[\text{Fe}/\text{H}] \leq -1.0$) and can be compared to our MC results. To this data set, we have added additional determinations of R_b from studies which presented high quality luminosity functions of the globular clusters M3 (Rood et al. 1999), M5 (Sandquist et al. 1996), M10 (Pollard et al. 2005), M12 (Hargis et al. 2004). Each of these observational studies presented luminosity functions based upon observations of $> 10,000$ stars in a given cluster. The

comparison between these data and the MC models is shown in Figure 6, assuming the Zinn & West (1984) metallicity scale. For this metallicity scale our theoretical predication has a reduced $\chi^2 = 1.23$ when compared to the observations. This implies that our models provide a reasonable fit to the observations. Formally, this value of a reduced χ^2 implies that the models have a 14% probability of correctly describing the data. If the Carretta & Gratton (1997) metallicity scale is used, then the reduced $\chi^2 = 1.34$ (6.5% probability) and the models provide an acceptable fit to the data.

The observed luminosity function of M10 was found to disagree with the predications of standard stellar evolution theory (Pollard et al. 2005), due to the fact that there are too many stars on the RGB compared to the main-sequence. From the Pollard et al. (2005) luminosity function, M10 has $R_b = 0.55 \pm 0.10$, compared to a predicted value of $R_b = 0.49 \pm 0.01$ on the Carretta & Gratton (1997) metallicity scale and $R_b = 0.48 \pm 0.01$ on the Zinn & West (1984) metallicity scale. Thus, the excess number of stars on the main-sequence has not lead to an anomalous number of stars in the bump region on the RGB.

7. Summary

We use a large Monte Carlo simulation to investigate theoretical uncertainties in the RGB luminosity function, specifically in the V -band magnitude of the red giant bump and excess number of stars in the bump. We find excellent agreement between theoretical and observational values for the bump magnitude, with the uncertainty in theoretical values comparable to the scatter in observational values. Metallicity has a very significant effect on the bump magnitude, while the cluster age impacts the bump magnitude at a level lower than the theoretical uncertainties. The most important sources of uncertainty in the predication of the bump magnitude are the alpha-capture overabundance $[\alpha/\text{Fe}]$, the mixing length, low-temperature opacities, and the treatment of surface boundary conditions. Theoretical uncertainties in stellar evolution models have little impact on the excess number of stars in the bump region. This is a robust prediction of standard stellar evolution is found to be in reasonable agreement with observations.

Research supported in part by a NSF CAREER grant 0094231 to Brian Chaboyer. Dr. Brian Chaboyer is a Cottrell Scholar of the Research Corporation.

REFERENCES

- Adelberger, E. C., et al. 1998, *Reviews of Modern Physics*, 70, 1265
- Alexander, D. R. & Ferguson, J. W. 1994, *ApJ*, 437, 87
- Alongi, M., Bertelli, G., Bressan, A., & Chiosi, C. 1991, *A&A*, 244, 95

- Basu, S., Pinsonneault, M. H., & Bahcall, J. N. 2000, *ApJ*, 529, 1084
- Bolte, M. 1994, *ApJ*, 431, 223
- Bono, G., Cassisi, S., Zoccali, M., & Piotto, G. 2001, *ApJ*, 546, L109
- Braaten, E. & Segel, D. 1993, *Phys. Rev. D*, 48, 1478
- Canuto, V. 1970, *ApJ*, 159, 641
- Carretta, E. & Gratton, R. G. 1997, *A&AS*, 121, 95
- Cassisi, S., degl’Innocenti, S., & Salaris, M. 1997, *MNRAS*, 290, 515
- Cassisi, S., Castellani, V., degl’Innocenti, S., & Weiss, A. 1998, *A&AS*, 129, 267
- Cassisi, S. & Salaris, M. 1997, *MNRAS*, 285, 593
- Castellani, V. & degl’Innocenti, S. 1993, *ApJ*, 402, 574
- Castellani, V. & degl’Innocenti, S. 1999, *A&A*, 344, 97
- Catelan, M., de Freitas Pacheco, J. A., & Horvath, J. E. 1996, *ApJ*, 461, 231
- Caughlan, G. R. & Fowler, W. A. 1988, *Atomic Data and Nuclear Data Tables*, 40, 283
- Chaboyer, B., Demarque, P., Kernan, P. J., & Krauss, L. M. 1996, *Science*, 271, 957
- Chaboyer, B., Demarque, P., Kernan, P. J., & Krauss, L. M. 1998, *ApJ*, 494, 96
- Chaboyer, B., Fenton, W. H., Nelan, J. E., Patnaude, D. J., & Simon, F. E. 2001, *ApJ*, 562, 521
- Chaboyer, B. & Kim, Y. 1995, *ApJ*, 454, 767
- Chaboyer, B. & Krauss, L. M. 2002, *ApJ*, 567, L45
- Christensen-Dalsgaard, J., Proffitt, C. R., & Thompson, M. J. 1993, *ApJ*, 403, L75
- Clayton, D. D. 1968, *Principles of Stellar Evolution and Nucleosynthesis* (New York: McGraw-Hill)
- Fusi Pecci, F., Ferraro, F. R., Crocker, D. A., Rood, R. T., & Buonanno, R. 1990, *A&A*, 238, 95
- Graboske, H. C., Dewitt, H. E., Grossman, A. S., & Cooper, M. S. 1973, *ApJ*, 181, 457
- Green, E. M., Demarque, P., & King, C. R. 1987, *The revised Yale isochrones and luminosity functions* (New Haven: Yale Observatory)
- Guenther, D. B., Demarque, P., Kim, Y.-C., & Pinsonneault, M. H. 1992, *ApJ*, 387, 372
- Haft, M., Raffelt, G., & Weiss, A. 1994, *ApJ*, 425, 222

- Hargis, J. R., Sandquist, E. L., & Bolte, M. 2004, *ApJ*, 608, 243
- Hubbard, W. B. & Lampe, M. 1969, *ApJS*, 18, 297
- Iglesias, C. A. & Rogers, F. J. 1996, *ApJ*, 464, 943
- Itoh, N., Hayashi, H., Nishikawa, A., & Kohyama, Y. 1996, *ApJS*, 102, 411
- Itoh, N., Mitake, S., Iyetomi, H., & Ichimaru, S. 1983, *ApJ*, 273, 774
- Krauss, L. M. & Chaboyer, B. 2003, *Science*, 299, 65
- Krishna Swamy, K. S. 1966, *ApJ*, 145, 174
- Kurucz, R. L. 1979, *ApJS*, 40, 1
- Langer, G. E., Bolte, M., & Sandquist, E. 2000, *ApJ*, 529, 936
- Mitake, S., Ichimaru, S., & Itoh, N. 1984, *ApJ*, 277, 375
- Mitler, H. E. 1977, *ApJ*, 212, 513
- Pollard, D. L., Sandquist, E. L., Hargis, J. R., & Bolte, M. 2005, *ApJ*, 628, 729
- Raffelt, G. G. 1990, *ApJ*, 365, 559
- Raffelt, G. & Weiss, A. 1992, *A&A*, 264, 536
- Riello, M. et al. 2003, *A&A*, 410, 553
- Rogers, F. J. 1994, in *IAU Colloq. 147, The Equation of State in Astrophysics*, ed. G. Chabrier & E. Schatzman (Cambridge: Cambridge Univ. Press), 16
- Rood, R. T. et al. 1999, *ApJ*, 523, 752
- Salaris, M., Cassisi, S., & Weiss, A. 2002, *PASP*, 114, 375
- Salpeter, E. E. 1954, *Australian J. Phys.*, 7, 353
- Salpeter, E. E. 1955, *ApJ*, 121, 161
- Sandquist, E. L., Bolte, M., Stetson, P. B., & Hesser, J. E. 1996, *ApJ*, 470, 910
- Singh, H. P., Roxburgh, I. W., & Chan, K. L. 1998, *A&A*, 340, 178
- Sweigart, A. V. 1973, *A&A*, 24, 459
- Thoul, A. A., Bahcall, J. N., & Loeb, A. 1994, *ApJ*, 421, 828
- Vandenberg, D. A. & Bell, R. A. 1985, *ApJS*, 58, 561

Vandenberg, D. A., Larson, A. M., & de Propris, R. 1998, *PASP*, 110, 98

Weiss, A. & Salaris, M. 1999, *A&A*, 346, 897

Zinn, R. & West, M. J. 1984, *ApJS*, 55, 45

Zoccali, M., Cassisi, S., Piotto, G., Bono, G., & Salaris, M. 1999, *ApJ*, 518, L49

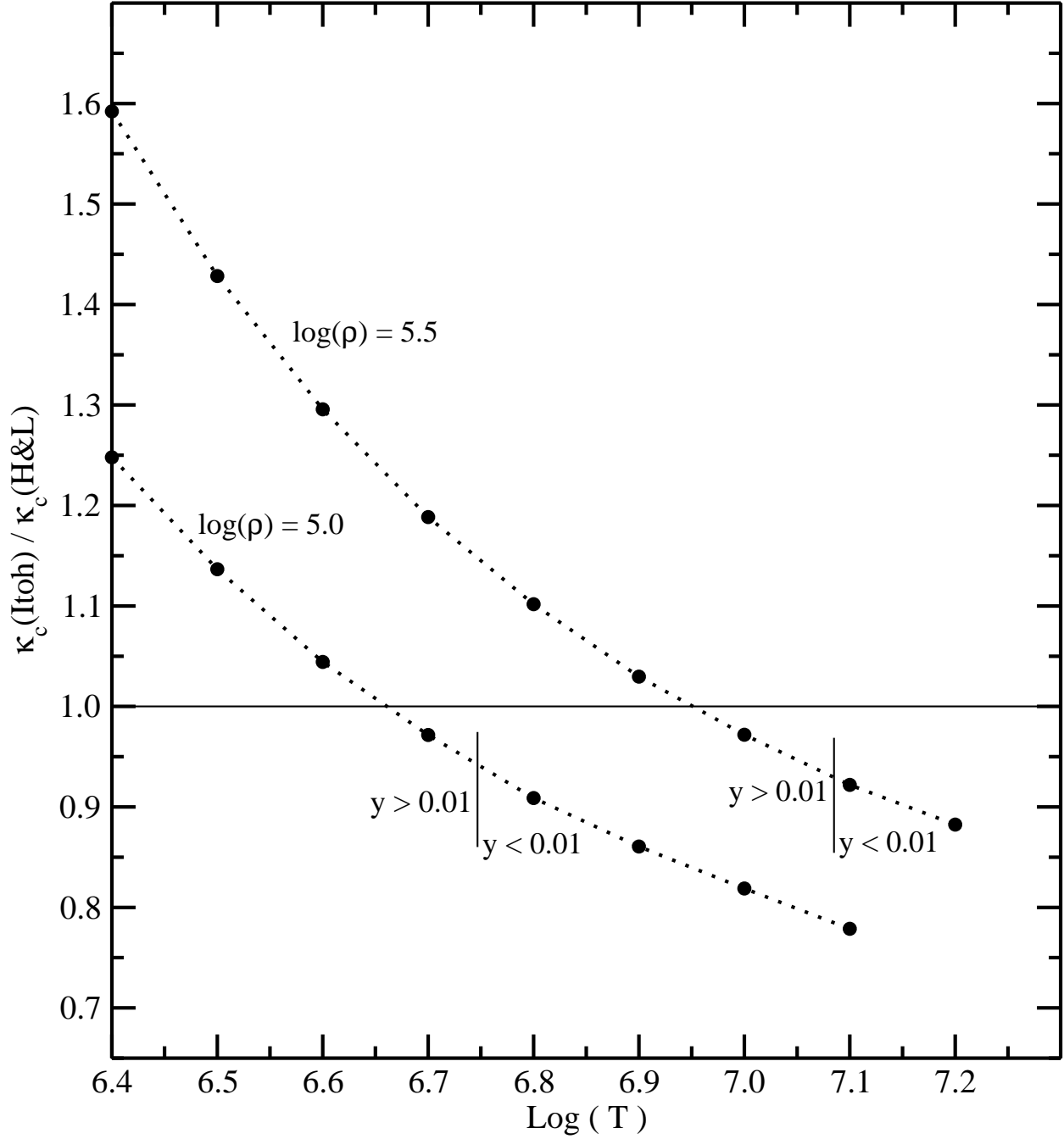


Fig. 1.— The fractional difference between the conductive opacities of Itoh et al. (1983) and Hubbard & Lampe (1969).

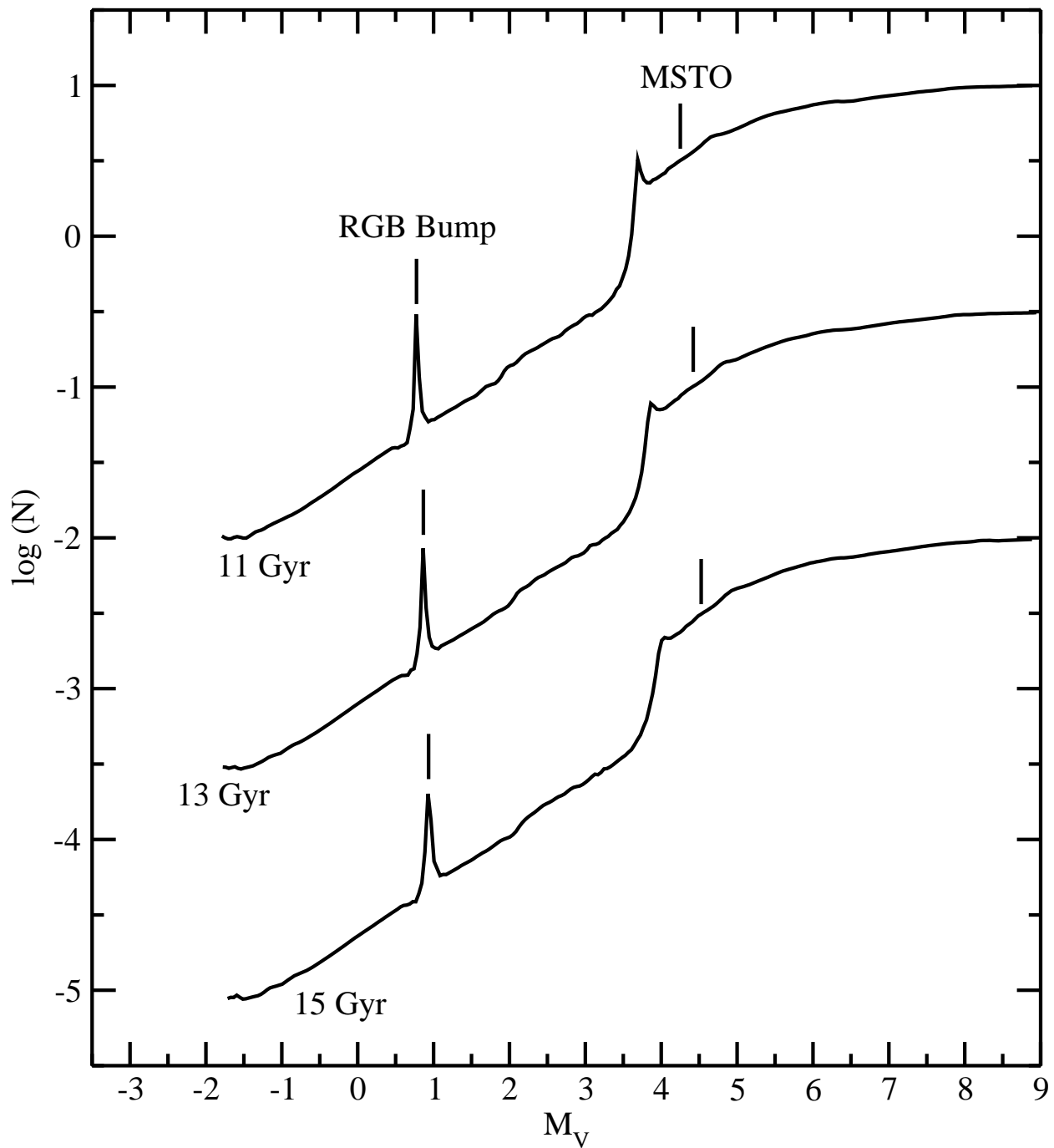


Fig. 2.— Luminosity functions calculated using a value for each stellar evolution parameter from the center of its uncertainty range, $[\text{Fe}/\text{H}] = -1.0$ and using the Salpeter IMF $\alpha = 2.35$. The location of the RGB bump and the main sequence turn-off point are indicated.

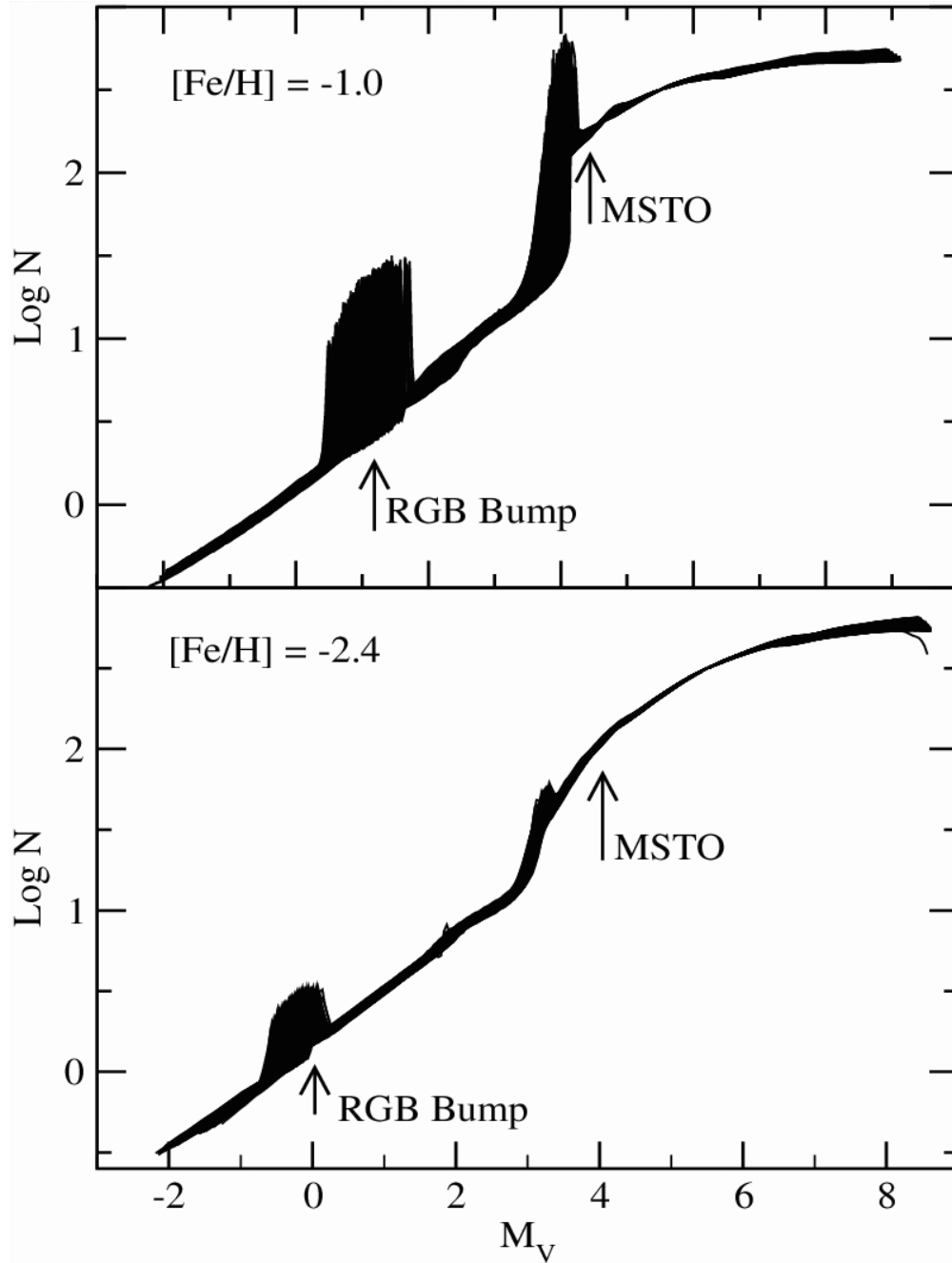


Fig. 3.— Monte Carlo luminosity functions calculated using the Salpeter IMF $\alpha = 2.35$, an age of 13 Gyr and $[\text{Fe}/\text{H}] = -1.0$ (upper panel) and $[\text{Fe}/\text{H}] = -2.4$ (lower panel).

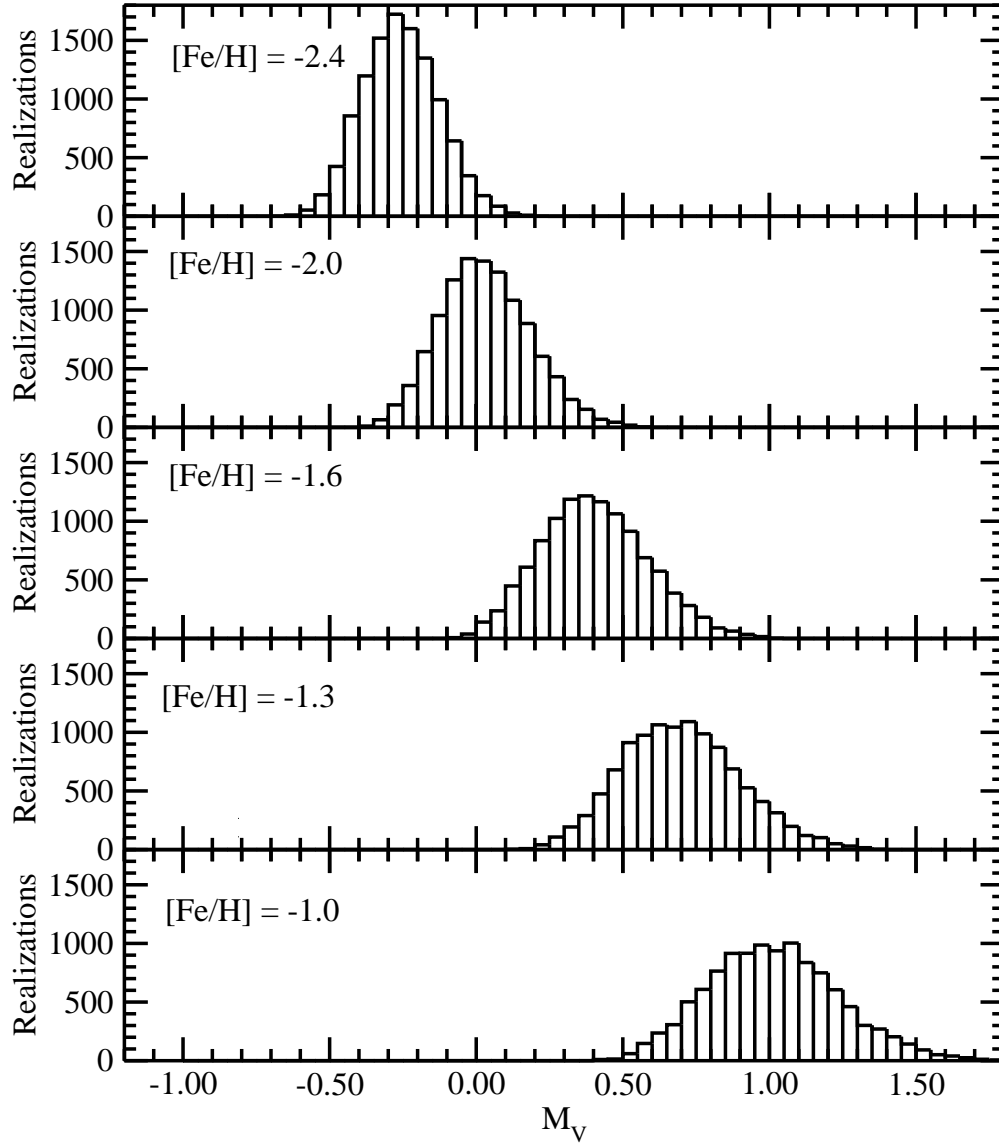


Fig. 4.— The distribution of RGB bump magnitudes at age 13 Gyr.

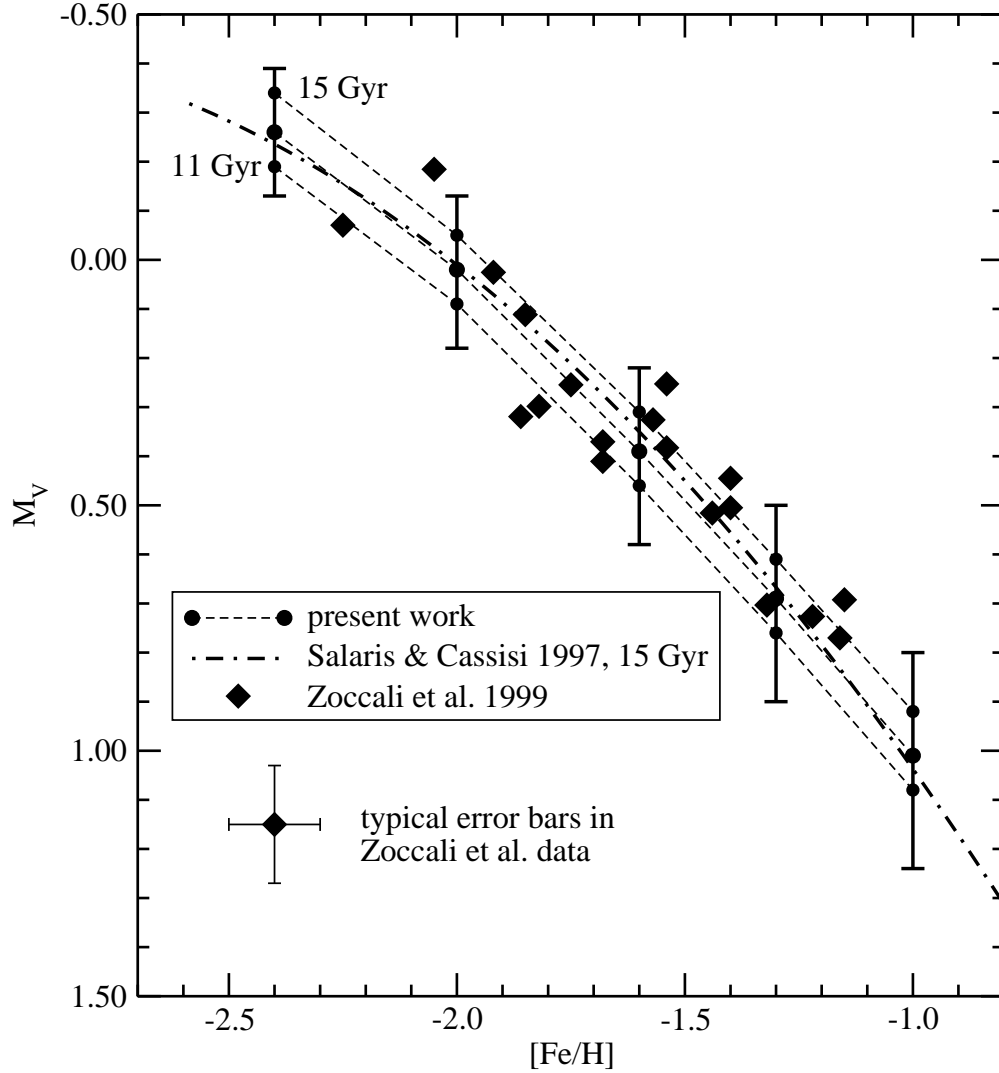


Fig. 5.— M_V -band magnitude of the RGB bump as a function of metallicity for the ages of 11, 13 and 15 Gyr. The error bars represent correlated 68% confidence limits in our results, are shown only for age 13 Gyr. The same confidence limits apply at all ages. Also shown is the theoretical relation of Cassisi & Salaris (1997). The observational results of Zoccali et al. (1999) assuming the globular cluster distance scale of Krauss & Chaboyer (2003). Each observational point has an associated uncertainty of approximately ± 0.10 dex in $[Fe/H]$ and ± 0.12 mag in M_V .

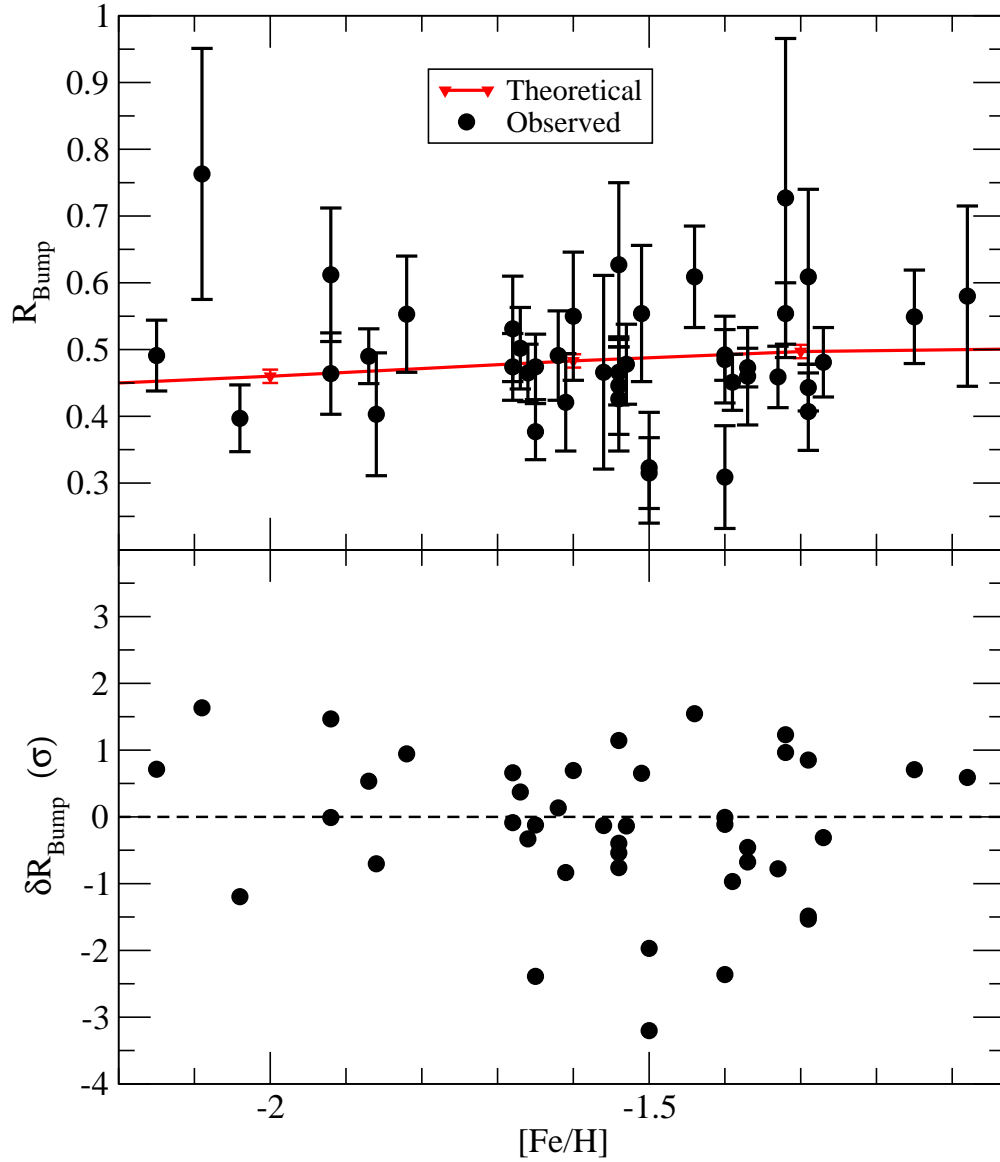


Fig. 6.— Comparison between R_b predicted by theory and observations (see text for references) as a function of the Zinn & West (1984) metallicity. The bottom panel is the residuals between the theoretical relation and the observations. These residuals have been normalized by dividing the actual residual by the error in each of individual observations added in quadrature with the error in the theoretical prediction.

Table 1. Stellar Evolution Parameters in the Monte Carlo Simulation.

Parameter	Standard	Distribution	Type
He mass fraction (Y)	n/a	0.245 – 0.250	unif.
$[\alpha/\text{Fe}]$	n/a	0.2 – 0.7 dex	unif.
Mixing length	n/a	$1.85 \pm 0.25 H_p$	gaus.
Convective overshoot	n/a	0.0 – 0.2 H_p	unif.
Atmospheric $T(\tau)$	grey or Krishna-Swamy (1966)	50/50	binary
Low-T opacities	Alexander & Ferguson (1994)	0.7 – 1.3	unif.
High-T opacities	Iglesias & Rogers (1996)	$1.00 \pm 2\%$ ($T \geq 10^7 \text{K}$) $0.98 \pm 4\%$ ($T \leq 10^6 \text{K}$)	gaus.
Diffusion coefficients	Thoul, Bahcall & Loeb (1994)	0.5 – 1.3	unif.
$p + p \rightarrow {}^2\text{H} + e^+ + \nu_e$	Adelberger et al. (1998)	$1 \pm 0.2\%$	gaus.
${}^3\text{He} + {}^3\text{He} \rightarrow {}^4\text{He} + 2p$	Adelberger et al. (1998)	$1^{+0.14\% +2.0\%}_{-0.09\% -1.2\%}$	unif.
${}^3\text{He} + {}^4\text{He} \rightarrow {}^7\text{Be} + \gamma$	Adelberger et al. (1998)	$1 \pm 6\%$	gaus.
${}^3\text{He} + {}^4\text{He} \rightarrow {}^7\text{Be} + \gamma$	Adelberger et al. (1998)	$1 \pm 3.2\%$	gaus.
${}^{12}\text{C} + p \rightarrow {}^{13}\text{N} + \gamma$	Adelberger et al. (1998)	$1 \pm 15\%$	gaus.
${}^{13}\text{C} + p \rightarrow {}^{14}\text{N} + \gamma$	Adelberger et al. (1998)	$1 \pm 15\%$	gaus.
${}^{14}\text{N} + p \rightarrow {}^{15}\text{O} + \gamma$	Adelberger et al. (1998)	$1 \pm 12\%$	gaus.
${}^{16}\text{O} + p \rightarrow {}^{17}\text{F} + \gamma$	Adelberger et al. (1998)	$1 \pm 16\%$	gaus.
Triple- α reaction rate	Caughlan & Fowler (1988)	$1 \pm 15\%$	gaus.
Neutrino cooling rate	Haft, Raffelt & Weiss (1994)	$1 \pm 5\%$	gaus.
Conductive opacities	Hubbard & Lampe (1969)	$1 \pm 20\%$	gaus.
BC_V	Green, Demarque & King (1987)	± 0.05 mag	unif.

Note. — Parameters in the lower portion of the table represent multiplicative or additive factors modifying standard tables or formulas. The atmospheric $T(\tau)$ relation is handled as a discrete choice between two independent formulas.

Table 2. Absolute V Magnitude of the Red Giant Bump

[Fe/H]	Median M_V					Confidence limits	
	11 Gyr	12 Gyr	13 Gyr	14 Gyr	15 Gyr	68%	95%
–2.4	–0.34	–0.30	–0.26	–0.22	–0.19	+0.13/ – 0.13	+0.27/ – 0.23
–2.0	–0.05	–0.01	0.02	0.06	0.09	+0.16/ – 0.15	+0.32/ – 0.27
–1.6	0.31	0.35	0.39	0.43	0.46	+0.19/ – 0.17	+0.38/ – 0.32
–1.3	0.61	0.65	0.69	0.73	0.76	+0.21/ – 0.19	+0.42/ – 0.35
–1.0	0.92	0.97	1.01	1.04	1.08	+0.23/ – 0.21	+0.47/ – 0.39

Table 3. Effect of Significant Stellar Evolution Parameters on $M_{V,b}$

Parameter (X)	Range	[Fe/H]	$\frac{\Delta M_{V,b}}{\Delta X}$ ^a	$\Delta M_{V,b}$ ^b
[α /Fe]	0.2 – 0.7 dex	–2.4	0.53	0.21
		–2.0	0.65	0.26
		–1.6	0.81	0.33
		–1.3	0.88	0.36
		–1.0	0.96	0.39
Mixing length	$1.85 \pm 0.25 H_p$	–2.4	–0.23	0.15
		–2.0	–0.29	0.18
		–1.6	–0.35	0.22
		–1.3	–0.42	0.27
		–1.0	–0.50	0.32
Low-T opacities	0.7 – 1.3	–2.4	0.16	0.08
		–2.0	0.20	0.10
		–1.6	0.24	0.12
		–1.3	0.30	0.14
		–1.0	0.36	0.17
Convective overshoot	0.0 – 0.2 H_p	avg.	0.47	0.07
Atmospheric $T(\tau)$	Eddington / Krishna-Swamy	avg.	—	0.07
$^{13}\text{C} + p \rightarrow ^{14}\text{N} + \gamma$	1 ± 0.15	avg.	0.24	0.07
He diffusion coef.	0.5 – 1.3	avg.	0.09	0.06

^aThe slope of the $M_{V,b}$ -parameter dependence.

^bAmount by which the bump magnitude changes as the parameter varies across its 80% uncertainty range (see text for discussion).

Table 4. Confidence Limits on $M_{V,b}$ for a Fixed Individual Parameter

Parameter (X)	[Fe/H]	68% c.l.
[α /Fe]	–2.4	+0.10/ – 0.08
	–2.0	+0.12/ – 0.09
	–1.6	+0.14/ – 0.11
	–1.3	+0.15/ – 0.12
	–1.0	+0.18/ – 0.13
Mixing length	–2.4	+0.12/ – 0.10
	–2.0	+0.15/ – 0.12
	–1.6	+0.18/ – 0.14
	–1.3	+0.19/ – 0.15
	–1.0	+0.20/ – 0.17
Low-T opacities	–2.4	+0.12/ – 0.11
	–2.0	+0.15/ – 0.14
	–1.6	+0.18/ – 0.17
	–1.3	+0.20/ – 0.19
	–1.0	+0.22/ – 0.21

Table 5. Median R_b Values

[Fe/H]	Average	11 Gyr	12 Gyr	13 Gyr	14 Gyr	15 Gyr
–2.4	0.44	0.45	0.45	0.44	0.43	0.43
–2.0	0.46	0.47	0.47	0.46	0.45	0.45
–1.6	0.48	0.50	0.49	0.48	0.48	0.47
–1.3	0.50	0.51	0.50	0.50	0.49	0.49
–1.0	0.50	0.51	0.50	0.50	0.50	0.50

Note. — In all cases the 68% confidence level is ± 0.01 and the 95% confidence level is ± 0.02 .

Table 6. Impact of Significant Stellar Evolution Parameters on R_b .

Parameter (X)	Range	[Fe/H]	$\frac{\Delta R_b}{\Delta X}$ ^a	ΔR_b ^b
[α /Fe]	0.2 – 0.7 dex	–2.4	0.032	0.013
		–2.0	0.041	0.017
		–1.6	0.043	0.018
		–1.3	0.009	0.004
		–1.0	–0.028	0.011
Mixing length	$1.85 \pm 0.25 H_p$	avg.	0.015	0.010
High-T opacities	1 ± 0.02	–1.3 to –2.4	0.12	0.006
He diffusion	0.5 – 1.3	–1.3 to –2.4	0.008	0.005
Low-T opacities	0.7 – 1.3	avg.	–0.009	0.004

^aSlope of the R_b -parameter dependence.

^bAmount by which R_b changes as the parameter varies across its 80% uncertainty range.